Synthesis and Photoelectric Properties of Cu_2ZnGeS_4 and $Cu_2ZnGeSe_4$ Single-Crystalline Nanowire Arrays

Liang Shi,*,[†] Peiqun Yin,[†] Haojun Zhu,[‡] and Quan Li[‡]

[†]Department of Chemistry, University of Science and Technology of China, Hefei 230026, P. R. China.
[‡]Department of Physics, The Chinese University of Hong Kong, Shatin, New Territory, Hong Kong, P. R. China

ABSTRACT: Cu_2ZnGeS_4 (CZGS) and $Cu_2ZnGeSe_4$ (CZGSe) single crystalline nanowire arrays have been prepared via a convenient one-step nanoconfined solvothermal approach. The porous anodic aluminum oxide was used as a morphology directing template by offering nanospace in the AAO pores for confined solvothermal reaction. The structure, morphology, composition, and optical absorption properties of the as-prepared samples were characterized using X-ray powder diffraction, transmission electron microscopy, energy dispersive X-ray spectrometry, scanning electron microscopy, and a UV−vis spectrophotometer. The CZGS and CZGSe films are found to have obvious photoelectric response, indicating their potential in the application of photovoltaic devices.
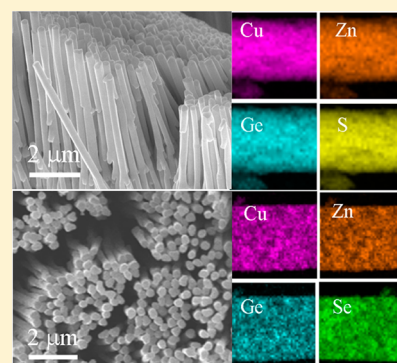
1. INTRODUCTION

Copper-based quaternary I_2−II−IV−VI_4 semiconductors have attracted much attention recently for their various excellent optical and electrical properties and potential application as solar-cell absorbers, photocatalysts for solar water splitting, and thermoelectric materials.[1−9] Cu_2ZnGeS_4 (CZGS) and $Cu_2ZnGeSe_4$ (CZGSe) belong to the family of Cu-based quaternary chalcogenide compounds. Both CZGS and CZGSe are reported experimentally and theoretically to be p-type semiconductors with bandgaps (E_g = 1.2 and ∼2.1 eV, respectively) that match the preferred range of solar irradiation and make them alternative indium- and cadmium-free absorber material for photovoltaic devices.[10−12] Over the past several years, many studies have been performed on the preparation, structure, and electronic properties of the quaternary I_2−II−IV−VI_4 chalcogenide semiconductors, including Cu_2ZnSnS_4, $Cu_2ZnSnSe_4$, $Cu_2ZnSnS_xSe_{4−x}$, $Cu_2CdSnSe_4$, and Ag_2ZnSnS_4.[13−19] However, relatively few investigations about CZGS and CZGSe have been conducted.[20−22]

The fabrication of arrays of well-aligned one-dimensional semiconductor nanostructure (nanowire, nanotube, or nanorod) are highly desirable because it is a key step toward building functional nanodevices such as nanoscale electronics and molecular sensing. Single crystalline semiconductor nanowire arrays have previously been prepared by various approaches. For example, the hydrothermal or solvothermal method has been reported to prepared single crystalline ZnS, ZnSe, and Co_3O_4 nanowire array.[23−25] The chemical vapor deposition approach has been used to synthesize ZnO, InSb, and GaN single crystalline nanowire array.[26−28] To the best of our knowledge, the single crystalline CZGS and CZGSe nanowire array configuration has not been reported. Such semiconductors in the ordered nanowire shape can offer a well-defined nanoscale domain with clearly identifiable grain boundaries, where an energy barrier could better avoid the charge carrier recombination.[29,30] Furthermore, continuous charge carrier transport pathways without dead ends may exist in the well-aligned nanowires. These favorable characteristics would lead to increase in conversion efficiency in nanowires photovoltaic devices. In spite of this, it is usually difficult to control the nucleation and growth of CZGS and CZGSe for fabrication of well-aligned nanostructures due to their very complicated phase diagrams. In addition, nanoscale materials show more phase complexity than their corresponding bulk materials. To date, it remains still a challenge for synthesis of CZGS and CZGSe nanowire arrays.

Recently, it has been reported that chemical reactions conducted within confined nanospaces exhibit distinct properties compared to the same processes involving macroscopic systems. The resulting nanoconfinement effect may lead to higher degree of stability and more favorable thermodynamic properties[31−33] In particular, as a result of nanoconfinement effect, reactions may occur under milder conditions; particle agglomeration and phase segregation can be avoided, and tailoring the particle shape and size becomes more available by choosing an appropriate template. Usually, nanoporous materials are utilized as templates to provide nanospace in the pores for nanoconfined chemical reactions. Among various types of templates, porous anodic aluminum oxide (AAO) is a particularly desirable hard template due to its advantages including monodisperse size distribution, high pore density, nearly parallel porous structures, and easily controlled pore

diameter.[34,35] Most importantly, AAO templates are thermally and mechanically stable; hence, they can be employed in rigorous reaction conditions. Inspired by the good properties of nanoconfined chemical reactions and AAO template, we here develop a nanoconfined solvothermal approach within AAO pores and first synthesized arrays of ordered uniform single crystalline CZGS and CZGSe nanowires. During the reaction process, AAO acted as a morphology directing template by offering nanospace in the AAO pores for nanoconfined solvothermal reaction. In addition, a film made of as-synthesized CZGS or CZGSe nanowires was found to have obvious photoelectric response, which indicates the potential use of them in solar energy conversion systems, such as the fabrication of photovoltaic devices.

2. EXPERIMENTAL SECTION

All reagents are analytical grade and used without further purification. AAO templates (Whatman Co., U.K.) with pore sizes of 200 nm in diameter were used in the experiments. For CZGS synthesis, the precursor solution contains 0.1 g of sulfur, 0.14 g of anhydrous $Cu(I)Cl$, 0.1 g of $ZnCl_2$, 120 μL of germanium(IV) methoxide, and 15 mL of anhydrous ethylenediamine (En). In the case of CZTSe, 0.23 g of selenium powder is used instead of sulfur; other conditions remained unchanged. In a typical procedure, a precursor solution (for CZGS or CZGSe) was prepared first with mild magnetic stirring. The AAO template was then immersed in the precursor solution, followed by 5 min sonication to remove the air in the AAO pore. Afterward, the system was attached to a Schlenk line to purge oxygen and water under rough vacuum, followed by 10 min nitrogen bubbling. The evacuation and N_2 bubbling process was cycled for three times at room temperature. The solution was then transferred into a 20 mL stainless steel Teflon-lined autoclave. The autoclave was sealed, and the temperature was maintained at 220 °C for 36 h before being cooled down to room temperature. The AAO template containing the product was taken out, thoroughly washed with ethanol and distilled water, and air-dried before characterization.

The overall crystallinity of the product was examined by X-ray diffraction (XRD, Rigakau RU-300 with Cu Kα radiation). The general morphology of the products was characterized using scanning electron microscopy (FESEM QF400). Detailed microstructure analysis was carried out using transmission electron microscopy (TEM Tecnai 20ST). The chemical composition and the spatial distribution of the compositional elements in the product were examined using an energy dispersive X-ray (EDX) spectrometer and Gatan image filtering (GIF) system, attached to the same microscope. For the SEM measurements, several drops of 1 M NaOH aqueous solution were added onto the sample to dissolve some part of the AAO template. The residual solution on the surface of the template was rinsed with distilled water. For the TEM and HRTEM measurements, the template was completely dissolved in 2 M NaOH aqueous solution. The product was centrifuged, thoroughly washed with distilled water to remove residual NaOH, and then rinsed with absolute ethanol. The UV–vis spectrum of the product was recorded in a UV–vis spectrophotometer (UV-1601PC, Shimadzu Corporation). $I-V$ curves were measured by linear sweep voltammetry on CH Instrument 660C electrochemical analyzer. A photoresponse device structure was fabricated to study the optoelectronic properties of the as-synthesized nanowires. The fabrication details of the device structure are as follows: an insulating quartz substrate was used as the substrate and thoroughly washed with a mixed solution of deionized water, acetone, and 2-propanol under sonication for 30 min. RF sputtering of Au electrodes were then completed on insulating quartz substrates. The CZGS and CZGSe film were fabricated by dripping the concentrated nanowires methanol dispersion on the electrodes and the substrate and then drying it for 5 h at room temperature under ambient conditions. A postanneal process was conducted at 300 °C in an Ar atmosphere to improve substrate adhesion.

3. RESULTS AND DISCUSSION

The CZGS and CZGSe products were characterized by X-ray diffraction (XRD) to obtain information on crystal structure and phase composition. Both products are phase-pure as determined. A typical XRD pattern of the as-prepared CZGS is shown in Figure 1a. All diffraction peaks can be indexed to the
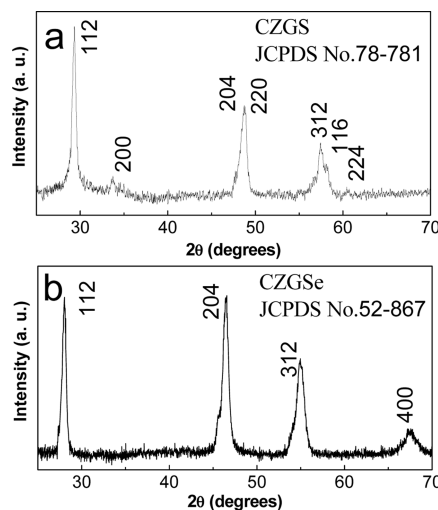
Figure 1. Representative XRD patterns of CZGS and CZGSe products.

tetragonal structured CZGS. After refinement, the lattice constant, $a = 5.268$ Å and $c = 10.537$ Å, is obtained, which matches well to the reported value for CZGS crystal (JCPDS card, No. 78-781). The XRD pattern of the CZGSe product is shown in Figure 1b, which can also be indexed to be tetragonal structure. The refined lattice constants of the CZGSe are $a = 5.603$ Å and $c = 11.045$ Å, in accordance with the reported value for CZGSe crystal (JCPDS card, No. 52-867). The broadening peaks in the two XRD patterns suggest that the grain sizes of the CZGS and CZGSe products are on a nanometer scale.

Figures 2a and 2e show respectively typical SEM images of as-prepared CZGS and CZGSe product with AAO template etched off, displaying that arrays made up of large-area dense nanowires with uniform diameter is formed. The average diameter of these nanowires is about 200 nm, being consistent with the pore size of the AAO template. The length of the nanowires is in the range of several micrometers. These CZGS and CZGSe nanowires are all found to be compact and parallel to each other, maintaining a nanowire array structure from the side view.

Detailed microstructure information and chemical composition of individual nanowire are obtained from TEM related studies including imaging, selected area electron diffraction (SAED), and energy dispersive X-ray spectrometry (EDX). A typical TEM image of straight nanowires in Figure 2b discloses that the CZGS nanowires are straight with smooth surface. SAED pattern (inset of Figure 2b) reveals clear symmetrical diffraction spots; in addition, the diffraction pattern did not change as the electron beam was moved along the nanowire, disclosing the uniform single crystalline nature of the CZGS nanowires. The EDX spectrum (Figure 2c) taken from the sample reveals intense peaks of Cu, Zn, Ge, and S, indicating the chemical composition of Cu, Zn, Ge, and S, only. The gold and carbon signals come from the supporting TEM grid. EDX
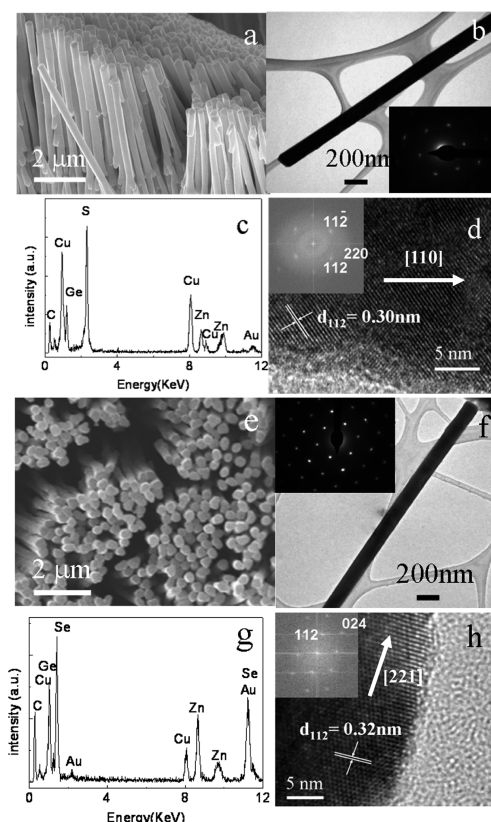
Figure 2. SEM (a), TEM (b), SAED (inset of b), and HRTEM (d) images and EDX spectrum (c) of the CZGS nanowires array. The inset of (d) shows a two-dimensional Fourier transform pattern of the lattice resolved image for CZGS nanowires. SEM (e), TEM (f), SAED (inset of f), and HRTEM (h) images and EDX spectrum (g) of the as-prepared CZGSe nanowire array. The inset of (h) shows a two-dimensional Fourier transform pattern of the lattice-resolved image CZGSe nanowires.

quantitative analysis gives an average Cu/Zn/Ge/S composition ratio of 2:1:1:4, in accordance with the stoichiometry of Cu_2ZnSnS_4. A high-resolution TEM (HRTEM) image shown in Figure 2d shows clear lattice spacing of 0.30 nm which corresponds well to the d spacing of the (112) planes in tetragonal chalcopyrite structured CZGS, confirming again the well-crystallized CZGS nanowires. The inset of Figure 2d shows a two-dimensional Fourier transform pattern of the lattice resolved image, which can be indexed to the $[1-10]$ zone of tetragonal structured CZGS. Carefully analysis of the HRTEM results showed that CZGS nanowires have an axial growth crystal plane of (220) and, accordingly, a growth axis in the [110] direction.

For CZGSe nanowires, the TEM image (Figure 2e) and its SAED pattern (inset of Figure 2e) display its single crystalline nature. The EDX spectrum (Figure 2g) exhibits its composition of Cu, Zn, Ge, and Se only. The HRTEM image shown in Figure 2h shows clear lattice spacing of 0.32 nm, matching well to the d spacing of the (112) planes in tetragonal structured CZGSe. The inset of Figure 2d discloses a two-dimensional Fourier transform pattern of the lattice resolved image, which can be indexed to the $[0-21]$ zone of tetragonal structured CZGSe. Based on the high-resolution image and its two-dimensional Fourier transform pattern, CZGSe nanowires are determined to have an axial growth crystal plane of (112) and a growth axis in the [221] direction.

STEM-EDX elemental mapping can provide information on the spatial distribution of different compositional elements in the CZGS and CZGSe nanowires. Figure 3a shows the dark
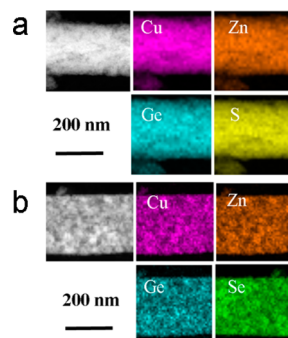
Figure 3. (a) Dark field image of a portion of CZGS nanowire and EDX elemental maps of Cu, Zn, Ge, and S. (b) Dark field image of a portion of CZGSe nanowire and EDX elemental maps of Cu, Zn, Ge, and Se.

field image of a portion of the CZGS single nanowire and gives the elemental maps of Cu, Zn, Ge, and S. It illustrates clearly that the spatial distribution of compositional elements in CZGS nanowires is uniform. Figure 3b also demonstrates that the spatial well-distributed Cu, Zn, Ge, and Se elements in CZGSe nanowires.

Both CZGS and CZGSe samples appear black due to their strong photon absorption in the entire visible range of light, suggesting their potential application as solar energy conversion materials. Figure 4 shows the room temperature UV−vis
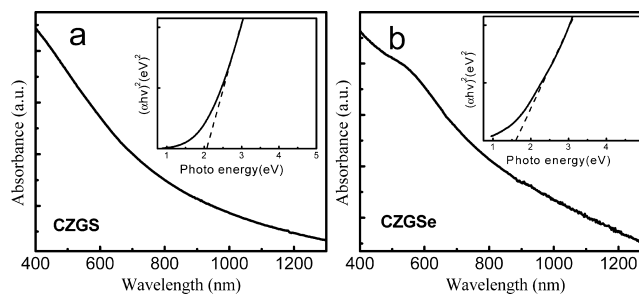
Figure 4. Typical room temperature UV−vis absorbance spectra of the CZGS and CZGSe nanowires.

absorption spectra for the as-prepared CZGS and CZGSe nanowires samples. Estimation on the optical band gap (E_g) of the CZGS and CZGSe nanowires can be obtained by plotting $(\alpha h\nu)^2$ as a function of the photon energy (in the inset of Figures 4a and 4b), with α being the absorption coefficient, h Planck's constant, and ν the frequency. Based on the intersection of the extrapolated linear portion, the E_g values can be calculated to be 2.05 eV for CZGS and 1.59 eV for CZGSe, in agreement with that of reported value for CZGS and CZGSe.[10,36] Such band gap values are desirable for the photovoltaic applications.

A possible formation mechanism of CZGS and CZGSe nanowires arrays can be proposed as follows. During the reaction process, we believe ethylenediamine plays an important role in the formation of nanocrystalline CZGS and CZGSe nanowires. Being a good solvent of sulfur or selenium powder, ethylenediamine dissolved them easily with stirring

after addition. During the reaction, ethylenediamine acted as both a chelating agent and a reducing agent. As a bidentate ligand, ethylenediamine chelated with Cu^+, Zn^{2+}, and Ge^{4+} to form complex ions with its five-membered-ring chelated structure, which was proved to be the most energetic stable among possible isomeric structures.[37] Because of the unique structure of ethylenediamine and the nanoconfined reaction environment, the generation of quaternary sulfides or selenides may be facilitated. Meanwhile, as a reducing agent, ethylenediamine reduced the dissolved elemental S or Se to negatively charged S^{2-} or Se^{2-} with an organic nucleophilic attack. S^{2-} or Se^{2-} reacted with complex ions (composed of the En chelated Cu^+, Zn^{2+}, Ge^{4+}) to form CZGS or CZGSe, then starting nucleation within AAO pores. In our present case, the solvothermal reaction and subsequent nucleation and crystal growth were all confined within the pores of AAO template in the medium of ethylenediamine; oxidation of product can be avoided effectively. In the nucleation stage, either homogeneous nucleation or heterogeneous nucleation is possible. Generally, heterogeneous nucleation on pore walls leads to polycrystalline materials in an AAO template aided synthesis.[38] But our product is single crystalline nanowires. So, heterogeneous nucleation did not likely happen. Therefore, a homogeneous nucleation should occur in our reaction. After nucleation, the crystal growth conducted within the channels of AAP template.

It is also found that long reaction duration is necessary for the formation of single crystalline nanowires. If the reaction was conducted for about 10 h, the product was polycrystalline nanowires composed of loosely packed nanoparticles. When the reaction was prolonged to 20 h, the nanoparticles in nanowires became denser. If the heating time was above 36 h, the final product turned to be single crystalline nanowires. Therefore, a polycrystalline-to-single crystalline evolution has occurred for the formation of CZGS and CZGSe nanowires. Here, oriented attachment mechanism can be used to explain the crystal growth process in which smaller particles with common crystallographic orientations directly combine together to form larger ones by crystallographic fusion at the planar interface. Similar behavior has happened for Cu_2ZnSnS_4 and $Cu_2ZnSnSe_4$ single crystalline nanowires.[13]

As a result of the confinement of the AAO pores, one-dimensional single crystalline nanowires with diameter determined by the pore size in the AAO template was generated, which is evidenced by the SEM and TEM characterization of our product.

To investigate the photoelectric properties, the current–voltage (I−V) measurements for CZGS film and CZGSe film were performed. Figure 5 shows the current–voltage (I−V) curves of the films tested in the darkness and under an illumination intensity of 100 mW/cm^2 from a 150 W xenon lamp (Bentham IL7), which was measured in a 1 V bias range. It is found that a promising increase of about 2.6 times for CZGS and 1.5 times for CZGSe in current at 1 V under light irradiation relative to the dark state. CZGS and CZGSe are known to be typically p-type. Light irradiation excites electrons in the valence band to the conduction band and then increases the holes in them. As a result, the current is increased obviously and the conductivity of the film is enhanced. This obvious photoresponsive behavior indicates the potential use of as-synthesized CZGS and CZGSe nanowires in solar energy conversion systems, such as the fabrication of photovoltaic devices.
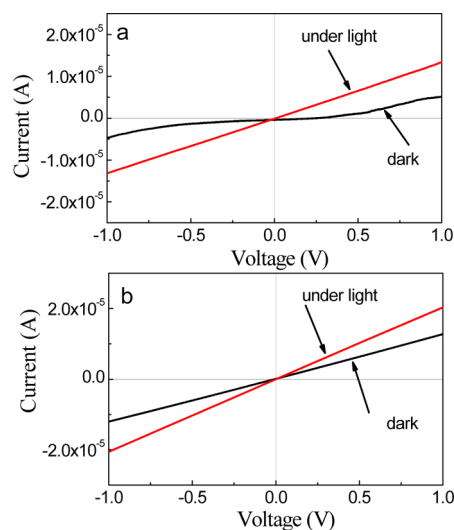
Figure 5. Current−potential (I−V) curve of the CZGS film (a) and CZGSe film (b) tested in the darkness (black line) and under illumination (red line).

4. CONCLUSIONS

In conclusion, single-crystalline nanowires arrays of quaternary CZGS and CZGSe have been synthesized through a simple nanoconfined solvothermal solution strategy within AAO nanopores. UV−vis absorption spectra revealed that the as-prepared CZGS and CZGSe nanowires have strong optical absorption in the visible region, and the band gaps match well with that of the corresponding bulk materials, disclosing their suitability for the photovoltaic application. The CZGS and CZGSe films have been fabricated and showed obviously enhanced conductivity under light irradiation. The as-prepared CZGS and CZGSe nanowires may be promising for use as light-absorption layers in solar cells as well as other nano-electronic devices, such as photoconducting cells and field-effect transistors.

■ AUTHOR INFORMATION

Corresponding Author
*Phone 86-551-3607234; Fax 86-551-3607402; e-mail sliang@ustc.edu.cn (L.S.).

Notes
The authors declare no competing financial interest.

■ REFERENCES

(1) Shavel, A.; Arbiol, J.; Cabot, A. Synthesis of quaternary chalcogenide nanocrystals: Stannite $Cu_2ZnxSn_ySe_{1+x+2y}$. *J. Am. Chem. Soc.* **2010**, *132*, 4514−4515.

(2) Ford, G. M.; Guo, Q.; Agrawal, R.; Hillhouse, H. W. Earth abundant element $Cu_2Zn(Sn_{1-x}Ge_x)S_4$ nanocrystals for tunable band gap solar cells: 6.8% efficient device fabrication. *Chem. Mater.* **2011**, *23*, 2626−2629.

(3) Weber, A.; Schmidt, S.; Abou-Ras, D.; Schubert-Bischoff, P.; Denks, I.; Mainz, R.; Schock, H. W. Texture inheritance in thin-film growth of Cu_2ZnSnS_4. *Appl. Phys. Lett.* **2009**, *95*, 041904.

(4) He, J.; Sun, L.; Chen, S.; Chen, Y.; Yang, P.; Chu, J. Composition dependence of structure and optical properties of $Cu_2ZnSn(S,Se)_4$

solid solutions: An experimental study. *J. Alloys Compd.* **2012**, *511*, 129−132.

(5) Scragg, J.; Dale, P.; Peter, L. Synthesis and characterization of Cu_2ZnSnS_4 absorber layers by an electrodeposition-annealing route. *Thin Solid Films* **2009**, *517*, 2481−2484.

(6) Chen, S. Y.; Yang, J. H.; Gong, X. G.; Walsh, A.; Wei, S. H. Intrinsic point defects and complexes in the quaternary kesterite semiconductor Cu_2ZnSnS_4. *Phys. Rev. B* **2010**, *81*, 245204.

(7) Ahn, S.; Jung, S.; Gwak, J.; Cho, A.; Shin, K.; Yoon, K.; Park, D.; Cheong, H.; Yun, J. H. Determination of band gap energy (E-g) of $Cu_2ZnSnSe_4$ thin films: On the discrepancies of reported band gap values. *Appl. Phys. Lett.* **2010**, *97*, 021905.

(8) Todorov, T. K.; Reuter, K. B.; Mitzi, D. B. High-efficiency solar cell with earth-abundant liquid-processed absorber. *Adv. Mater.* **2010**, *22*, E156−E159.

(9) Tanaka, K.; Oonuki, M.; Moritake, N.; Uchiki, H. Cu_2ZnSnS_4 thin film solar cells prepared by non-vacuum processing. *Sol. Energy Mater. Sol. Cells* **2009**, *93*, 583−587.

(10) Levcenco, S.; Dumcenco, D.; Huang, Y. S.; Tiong, K. K.; Du, C. H. Anisotropy of the spectroscopy properties of the wurtz-stannite Cu_2ZnGeS_4 single crystals. *Opt. Mater.* **2011**, *34*, 183−188.

(11) Matsushita, H.; Ichikawa, T.; Katsui, A. Structural, thermodynamical and optical properties of Cu_2-II-IV-VI_4 quaternary compounds. *J. Mater. Sci.* **2005**, *40*, 2003−2005.

(12) Chen, S.; Gong, X. G.; Walsh, A.; Wei, S. H. Electronic structure and stability of quaternary chalcogenide semiconductors derived from cation cross-substitution of II-VI and I-III-VI_2 compounds. *Phys. Rev. B* **2009**, *79*, 165211.

(13) Shi, L.; Pei, C. J.; Xu, Y. M.; Li, Q. Template-directed synthesis of ordered single-crystalline nanowires arrays of Cu_2ZnSnS_4 and $Cu_2ZnSnSe_4$. *J. Am. Chem. Soc.* **2011**, *133*, 10328−10331.

(14) Katagiri, H. Cu_2ZnSnS_4 thin film solar cells. *Thin Solid Films* **2005**, *480*, 426−432.

(15) Katagiri, H.; Saitoh, K.; Washio, T.; Shinohara, H.; Kurumadani, T.; Miyajima, S. Development of thin film solar cell based on Cu_2ZnSnS_4 thin films. *Sol. Energy Mater. Sol. Cells* **2001**, *65*, 141−148.

(16) Jimbo, K.; Kimura, R.; Kamimura, T.; Yamada, S.; Maw, W. S.; Araki, H.; Oishi, K.; Katagiri, H. Cu_2ZnSnS_4-type thin film solar cells using abundant materials. *Thin Solid Films* **2007**, *515*, 5997−5999.

(17) Fan, F. J.; Yu, B.; Wang, Y. X.; Zhu, Y. L.; Liu, X. J.; Yu, S. H.; Ren, Z. F. Colloidal synthesis of $Cu_2CdSnSe_4$ nanocrystals and hot-pressing to enhance the thermoelectric figure-of-merit. *J. Am. Chem. Soc.* **2011**, *133*, 15910−15913.

(18) Shi, L.; Li, Q. Thickness tunable $Cu_2ZnSnSe_4$ nanosheets. *CrystEngComm* **2011**, *13*, 6507−6510.

(19) Riha, S. C.; Parkinson, B. A.; Prieto, A. L. Compositionally tunable $Cu_2ZnSn(S_{1-x}Se_x)_4$ nanocrystals: Probing the effect of Se-inclusion in mixed chalcogenide thin films. *J. Am. Chem. Soc.* **2011**, *133*, 15272−15275.

(20) Chen, S. Y.; Walsh, A.; Luo, Y.; Yang, J. H.; Gong, X. G.; Wei, S. H. Wurtzite-derived polytypes of kesterite and stannite quaternary chalcogenide semiconductors. *Phys. Rev. B* **2010**, *82*, 195203.

(21) Zeier, W. G.; Londe, A. L.; Gibbs, Z. M.; Heinrich, C. P.; Panthöfer, M.; Snyder, G. J.; Tremel, W. Influence of a nano phase segregation on the thermoelectric properties of the p-type doped stannite compound $Cu_{2+x}Zn_{1-x}GeSe_4$. *J. Am. Chem. Soc.* **2012**, *134*, 7147−7154.

(22) Ibáñez, M.; Zamani, R.; LaLonde, A.; Cadavid, D.; Li, W. H.; Shavel, A.; Arbiol, J.; Morante, J. R.; Gorsse, S.; Snyer, G. J.; Cabot, A. $Cu_2ZnGeSe_4$ nanocrystals: Synthesis and thermoelectric properties. *J. Am. Chem. Soc.* **2012**, *134*, 4060−4063.

(23) Shi, L.; Xu, Y. M.; Li, Q. Shape-selective synthesis and optical properties of highly ordered one-dimensional ZnS nanostructures. *Cryst. Growth Des.* **2009**, *5*, 2214−2219.

(24) Shi, L.; Xu, Y. M.; Li, Q. Controlled fabrication of ZnSe arrays of well-aligned nanorods, nanowires, and nanobelts with a facile template-free route. *J. Phys. Chem. C* **2009**, *113*, 1795−1799.

(25) Xia, X. H.; Tu, J. P.; Zhang, Y. Q.; Mai, Y. J.; Wang, X. L.; Gu, C. D.; Zhao, X. B. Freestanding Co_3O_4 nanowire array for high performance supercapacitors. *RSC Adv.* **2012**, *2*, 1835−1841.

(26) Zhong, M.; Sato, Y.; Kurniawan, M.; Apostoluk, A.; Masenelli, B.; Maeda, E.; Ikuhara, Y.; Delaunay, J. J. ZnO dense nanowire array on a film structure in a single crystal domain texture for optical and photoelectrochemical applications. *Nanotechnology* **2012**, *23*, 495602.

(27) Wang, Y. N.; Chi, J. H.; Banerjee, K.; Grutzmacher, D.; Schapers, T.; Lu, J. G. Field effect transistor based on single crystalline InSb nanowire. *J. Mater. Chem.* **2011**, *21*, 2459−2462.

(28) Zhang, J.; Zhang, L. D.; Wang, X. F.; Liang, C. H.; Peng, X. S.; Wang, Y. W. Fabrication and photoluminescence of ordered GaN nanowire arrays. *J. Chem. Phys.* **2001**, *115*, 5714−5717.

(29) Peng, H.; Schoen, D. T.; Meister, S. X.; Zhang, F.; Cui, Y. Synthesis and phase transformation of In_2Se_3 and $CuInSe_2$ nanowires. *J. Am. Chem. Soc.* **2007**, *129*, 34−35.

(30) Hetzer, M. J.; Strzhemechny, Y. M.; Gao, M.; Contreras, M. A.; Zunger, A.; Brillson, L. J. Direct observation of copper depletion and potential changes at copper indium gallium diselenide grain boundaries. *Appl. Phys. Lett.* **2005**, *86*, 162105.

(31) Polak, M.; Rubinovich, L. Nanochemical equilibrium involving a small number of molecules: A prediction of a distinct confinement effect. *Nano Lett.* **2008**, *8*, 3543−3548.

(32) Liu, C. J.; Burghaus, U.; Besenbacher, F.; Wang, Z. L. Preparation and characterization of nanomaterials for sustainable energy production. *ACS Nano* **2010**, *4*, 5517−5526.

(33) Somorjai, G. A.; Frei, H.; Park, J. Y. Advancing the frontiers in nanocatalysis, biointerfaces, and renewable energy conversion by innovations of surface techniques. *J. Am. Chem. Soc.* **2009**, *131*, 16589−16605.

(34) Mallouk, T. E. Nanomaterials - stretching the mold. *Science* **2001**, *291*, 443−444.

(35) Mao, Y.; Wong, S. S. General, room-temperature method for the synthesis of isolated as well as arrays of single-crystalline ABO(4)-type nanorods. *J. Am. Chem. Soc.* **2004**, *126*, 15245−15252.

(36) Leon, M.; Levcenko, S.; Serna, R.; Gurieva, G.; Nateprov, A.; Merino, J. M.; Friedrich, E. J.; Fillat, U.; Schorr, S.; Arushanov, E. Optical constants of Cu_2ZnGeS_4 bulk crystals. *J. Appl. Phys.* **2010**, *108*, 093502.

(37) Alcamı, M.; Luna, A.; Mo, O.; Yanez, M.; Tortajada, J. Theoretical survey of the potential energy surface of ethylenediamine plus Cu^+ reactions. *J. Phys. Chem. A* **2004**, *108*, 8367−8372.

(38) Molares, M. E. T.; Buschmann, V.; Dobrev, D.; Neumann, R.; Scholtz, R.; Schuchert, I. U.; Vetter, J. Single-crystalline copper nanowires produced by electrochemical deposition in polymeric ion track membranes. *Adv. Mater.* **2001**, *13*, 62−65.